Title

Electron Paramagnetic Resonance and Magnetic Circular Dichroism Spectra of the Nitrogenase M Cluster Precursor Suggest Sulfur Migration upon Oxidation: A Proposal for Substrate and Inhibitor Binding.

Journal

Chembiochem : a European journal of chemical biology, 21(12)

ISSN

1439-4227

Authors

Rupnik, Kresimir
Tanifuji, Kazuki
Rettberg, Lee
et al.

Publication Date

2020-06-01

DOI

10.1002/cbic.201900681

Peer reviewed

HHS Public Access

Author manuscript

Chembiochem. Author manuscript; available in PMC 2021 June 15.

Published in final edited form as:

Chembiochem. 2020 June 15; 21(12): 1767–1772. doi:10.1002/cbic.201900681.

EPR and MCD spectra of the nitrogenase *M* cluster precursor suggest sulfur migration upon oxidation: A proposal for substrate and inhibitor binding

Kresimir Rupnik[a], **Kazuki Tanifuji**[b], **Lee Rettberg**[b], **Markus W. Ribbe**[b],[c], **Yilin Hu**[b], **Brian J. Hales**[a]

[a]Department of Chemistry, Louisiana State University, Baton Rouge, LA 70803

[b]Department of Molecular Biology & Biochemistry, University of California, Irvine, Irvine, CA 92697-3900 (USA)

[c]Department Chemistry, University of California, Irvine, Irvine, CA 92697-2025 (USA)

Abstract

The active site of the nitrogen fixing enzyme, Mo-nitrogenase, is the ***M*** cluster ([*MoFe*$_7$*S*$_9$*C*•*R-homocitrate*]), also known as the FeMo cofactor or FeMoco. The biosynthesis of this highly complex metallocluster involves a series of proteins. Among them, NifB, a radical-SAM enzyme, is instrumental in the assembly of the ***L*** cluster ([*Fe*$_8$*S*$_9$*C*]), a precursor and an all-iron core of the ***M*** cluster. In the absence of sulfite, NifB assembles a precursor form of the ***L*** cluster called the ***L**** cluster ([*Fe*$_8$*S*$_8$*C*]), which lacks the final 9th sulfur. EPR and MCD spectroscopies are used to probe the electronic structures of the paramagnetic, oxidized forms of both the ***L*** and ***L**** clusters, labeled ***L***^{Ox} and [***L****]^{Ox}, respectively. This study shows that both ***L***^{Ox} and [***L****]^{Ox} have nearly identical EPR and MCD spectra, suggesting that the two clusters have identical structures upon oxidation; in other words, a sulfur migrates away from ***L***^{Ox} following oxidation, rendering the cluster identical to [***L****]^{Ox}. It is proposed that a similar migration could occur to the ***M*** cluster upon oxidation and that it is an instrumental part of both ***M*** cluster formation and nitrogenase substrate/inhibitor binding.

Graphical Abstract

bhales@lsu.edu, yilinh@uci.edu, mribbe@uci.edu.

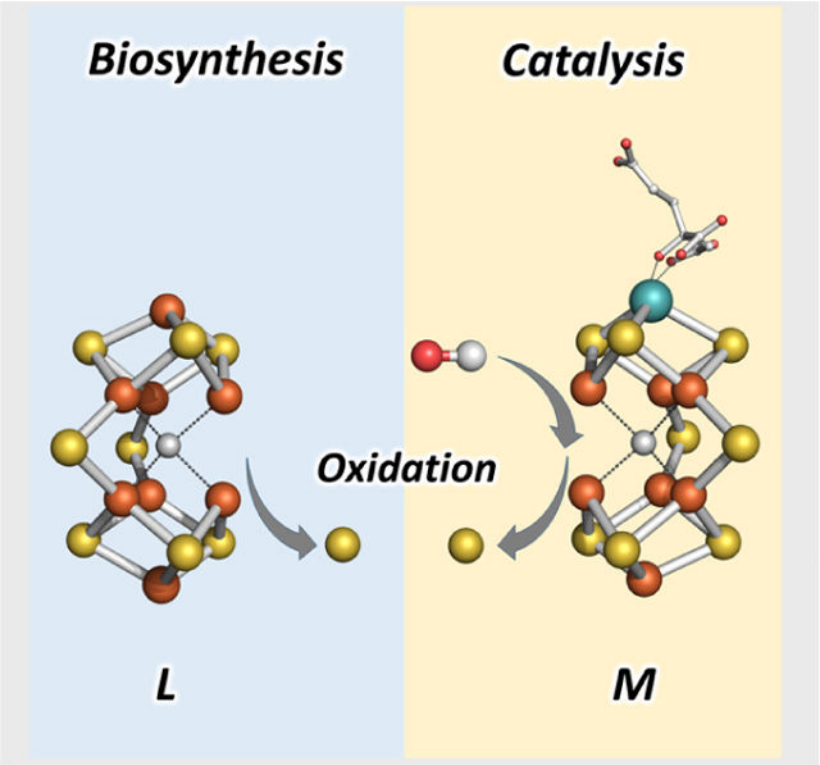

Combined EPR and MCD analyses show migration of a belt sulfur away from the nitrogenase cofactor precursor, ***L***, upon oxidation. A similar migration is proposed for the nitrogenase cofactor, ***M***, upon turnover. Such an oxidation-induced labilization of the cofactor belt region could be instrumental in nitrogenase cofactor biosynthesis and substrate/inhibitor binding.

Keywords

nitrogenase; M cluster; L cluster; magnetic circular dichroism; electron paramagnetic resonance

Introduction

The biological reduction of dinitrogen to ammonia is catalyzed by the enzyme nitrogenase. The best-characterized form of this enzyme, Mo-nitrogenase, contains two separable proteins: the Fe protein and the MoFe protein.[1] The latter protein contains two highly complex metalloclusters: the active-site ***M*** cluster, which is also called the FeMo cofactor or FeMoco ([$MoFe_7S_9C$•*R-homocitrate*]); and the ***P*** cluster ([Fe_8S_7]), which shuttles electrons from the Fe protein to the ***M*** cluster for substrate reduction.[2–8] Because of its complexity and central role in substrate reduction, the ***M*** cluster has received special attention regarding the mechanism of its formation. The biosynthesis of an all-Fe core of the ***M*** cluster occurs on NifB, a radical-SAM enzyme that contains three [Fe_4S_4] clusters.[9–11] One cluster ([Fe_4S_4]$_{SAM}$) is ligated to NifB through a *CxxCxxxC* motif that is characteristic of radical *S*-adenosyl-L-methionine (SAM) enzymes.[11,12] The remaining two transient [Fe_4S_4] clusters (***K*** cluster) are transformed into an [Fe_8S_9C] cluster (***L*** cluster, [Fe_8S_9C]) in a series

of radical SAM reactions, during which process the two 4Fe modules of the ***K*** cluster is fused into a single 8Fe ***L*** cluster concomitant with the insertion of a central carbide atom and a 9th sulfur atom. The ***L*** cluster represents the core structure of the ***M*** cluster except for the absence of Mo and homocitrate at one end of the cluster. Following its formation, the ***L*** cluster is transferred from NifB to NifEN, a scaffold protein, where Mo and homocitrate are inserted into the ***L*** cluster to yield a mature ***M*** cluster.[10]

Past investigations of the mechanism of the ***L*** cluster biosynthesis were hampered by the general instability of NifB isolates. An early successful step in characterizing NifB occurred when NifB was fused to NifEN to form a stable NifEN-B complex.[9] This complex was shown to be effective in inserting the central carbon into the fused ***K*** cluster to form the ***L*** cluster. ***Fe*** EXAFS studies of the ***L*** cluster on NifEN demonstrated that the ***Fe*** atom structural arrangement was the same as that of the ***M*** cluster.[13] A subsequent x-ray crystallographic study verified the similarity of the ***L*** and ***M*** clusters.[14] More recently, a stable form of NifB (*Ma*NifB) from a mesophilic methanogen, *Methanosarcina acetivorans*, was heterologously expressed in *Escherichia coli*, which now allows the study of the individual NifB protein.[15,16] *Ma*NifB is a monomer of ~38 kDa that is fully active in converting the ***K*** cluster to the ***L*** cluster upon incubation with SAM. Finally, the addition of the 9th sulfur atom in the ***L*** cluster has been shown to originate from sulfite.[17] Eliminating all external source of sulfite results in an incomplete 8-sulfur cluster precursor of the ***L*** cluster, designated the ***L**** cluster ([Fe_8S_8C]).[17,18]

To further probe the biosynthetic mechanism of the ***M*** cluster, a combined EPR and variable-temperature, variable-field magnetic circular dichroism (VTVH MCD) spectroscopic study was undertaken to characterize the precursors of the ***M*** cluster, the ***L*** and ***L**** clusters. This study reveals that both clusters, when oxidized, exhibit essentially identical EPR and MCD spectra, suggesting that they have identical structures. Implication of this finding is that the oxidized ***L*** cluster loses a sulfur atom, making it identical to the oxidized ***L**** cluster.

Results and Discussion

As outlined above, the biosynthesis of the ***M*** cluster involves a series of different Nif proteins. Among them, NifB is a radical SAM enzyme that serves as a scaffold for the assembly of the ***L*** cluster. Past studies suggested different spin states, paramagnetic[19,20] or diamagnetic,[21] for the ***L*** cluster in NifB. Regardless of its spin state in NifB, the ***L*** cluster extracted from NifB is paramagnetic,[20] exhibiting a near-axial EPR spectrum (g = [1.97, 1.83]) of an S = 1/2 spin system. The oxidized ***L*** cluster (***L^{Ox}***), either bound to or extracted from NifB, is also paramagnetic, exhibiting a single broad EPR signal (Figure 1a) centered at $g \sim 1.92$. [14,22,23]

The spin state of ***L^{Ox}*** has not yet been identified. In general, integer spin ***FeS*** clusters are often EPR-silent, especially in perpendicular mode. In those cases where they are EPR-active, they are normally high spin systems ($S \geq 3$) and typically exhibit inflections at X-band frequencies only at low field (high g-factors) corresponding to transitions between the highest ($\Delta m_s = 2S$) levels. By comparison, half-integer spin states are usually EPR-active,

especially when there is an inflection in the *g* 2 region of the spectrum. Considering all of this, $\boldsymbol{L^{Ox}}$ is likely a half-integer cluster.

As mentioned above, the ***L**** cluster ([Fe_8S_8C]) lacks the final 9 th *S* atom of the ***L*** cluster ([Fe_8S_9C]). In spite of this difference, the X-band EPR spectrum of the oxidized ***L**** cluster ([$\boldsymbol{L^*}]^{Ox}$) is essentially identical to that of $\boldsymbol{L^{Ox}}$ (Figure 1a).[17] Since both spectra are very broad, any possible underlying Zeeman structure cannot be identified. To help resolve the Zeeman structure, high frequency EPR spectroscopy is often used. Spectra recorded at different frequencies are best compared when plotted on the same *g*-factor scale. This is because *g*-factors are field dependent while line broadening is generally field independent.

The EPR spectrum of $\boldsymbol{L^{Ox}}$ recorded at W-band (94 GHz) (Figure 2) reveals no improved resolution, although there is a near-linear increase in the peak-to-peak ($\Delta \boldsymbol{B_{p\text{-}p}}$) line width at W-band ($\Delta \boldsymbol{B(W)_{p\text{-}p}}$ = 145 mT) compared to the line width at X-band ($\Delta \boldsymbol{B(X)_{p\text{-}p}}$ = 17 mT). There are several possibilities for the lack of improved resolution:

1. Since the linewidth is nearly linearly dependent on frequency, the spectrum is broadening at about the same rate as any possible *g*-factor splitting of an $S = 1/2$ spin system, leaving the spectrum essentially unchanged.
2. The spectrum represents only a single *g*-factor of an $S > 1/2$ spin system where the other *g*-factor signals are broadened beyond detection.

The increase in $\Delta \boldsymbol{B_{p\text{-}p}}$ with frequency suggests some structural variability (possibly *g*-strain) of $\boldsymbol{L^{Ox}}$ in NifB. The origin of this variability is unknown but may be related to the absence on $\boldsymbol{L^{Ox}}$ of homocitrate, a molecule that coordinates and, likely, stabilizes the ***M*** cluster in the MoFe protein.

Since the EPR spectra of $\boldsymbol{L^{Ox}}$ and $[\boldsymbol{L^*}]^{Ox}$ are not fully resolved, the electronic properties of these clusters cannot be characterized. Therefore, a VTVH MCD spectroscopic study was undertaken to probe their electronic structures. Figure 3 shows the MCD spectra of $\boldsymbol{L^{Ox}}$ and $[\boldsymbol{L^*}]^{Ox}$ in the range of 350–800 nm, recorded at a temperature of 1.4 K and a magnetic field of 6 T. The main feature of both spectra is a dominant, broad positive inflection maximizing at *ca.* 480 nm with a shoulder starting at *ca.* 410 nm and a minor positive inflection at *ca.* 717 nm. In general, as the structure of an ***FeS*** cluster becomes more complex, its MCD spectrum tends to broaden. For example, the nitrogenase ***M*** cluster and ***P*** cluster, which are clusters of comparable size to the ***L*** cluster, also exhibit broad MCD spectra.[24,25] Therefore, the broadness of the spectra in Figure 3 is not unexpected. The narrow, axial shape of the EPR spectrum of this cluster (Figure 1) is similar to that of an oxidized $[Fe_4S_4]^+$ cluster of *g* 2. However, the *g*-factor (1.92) and broad MCD spectral shape argue against this assignment.

What is unexpected is that the MCD spectrum of $[\boldsymbol{L^*}]^{Ox}$ (Figure 3) is essentially identical to that of $\boldsymbol{L^{Ox}}$. The MCD spectrum of an ***FeS*** cluster in the 350–800 nm wavelength region is dominated by $\boldsymbol{S \rightarrow Fe}$ charge-transfer bands. Since $[\boldsymbol{L^*}]^{Ox}$ lacks the 9th sulfur, one would expect its MCD spectrum to differ from that of $\boldsymbol{L^{Ox}}$. It doesn't. For a degenerate ground state, increasing the field (***B***) and/or decreasing the temperature (***T***) will increase the relative population of the lowest state, resulting in an increase in MCD spectral amplitude (Curie's

Law). Eventually, all of the paramagnetism will reside in the lowest state, at which point the MCD spectral amplitude will have reached a maximum (a situation termed saturation). The changes in the spectral amplitude of $\boldsymbol{L^{Ox}}$ and $[\boldsymbol{L^*}]^{\boldsymbol{Ox}}$ with field, monitored at 480 nm, are shown in Figure 4. Typical MCD amplitude curves exhibit a smooth increase from zero at $\boldsymbol{B} = 0$ to a maximum at saturation as $\boldsymbol{B}$ increases. The curves in Figure 4 are, therefore, atypical since they exhibit a near-linear upward break at around 3 T (dashed vertical line). This break occurs at approximately the same magnetic field for different temperatures, and it is observed in the cases of both clusters, which suggests that the spin system is not pure $S = 1/2$, as is implied by the g 1.92 EPR spectrum.

To identify spin states, magnetization curves are often constructed. A magnetization curve is a plot of the normalized MCD amplitude against $\boldsymbol{\beta B/2kT}$, where $\boldsymbol{\beta}$ is the Bohr magneton, $\boldsymbol{k}$ is the Boltzmann constant and $\boldsymbol{T}$ is the absolute temperature. The magnetization curves for $\boldsymbol{L^{Ox}}$ and $[\boldsymbol{L^*}]^{\boldsymbol{Ox}}$ are plotted In Figure 5 and, again, illustrate the unusual and atypical behavior observed at high field (Figure 4). Unfortunately, because of this atypical behavior, attempts to simulate the curves with different spin states and/or diamagnetic contributions using a program based on a previously reported procedure[26] proved fruitless. Therefore, the spin-state profile of these signals could not be identified.

Concept

In summary, $\boldsymbol{L^{Ox}}$ and $[\boldsymbol{L^*}]^{\boldsymbol{Ox}}$ exhibit nearly identical EPR and MCD spectra and magnetization curves. This is surprising since $\boldsymbol{L}$ and $\boldsymbol{L^*}$ are different clusters and, as such, would likely not have identical electronic structures. Either both the EPR and MCD spectra of $\boldsymbol{L^{Ox}}$ and $[\boldsymbol{L^*}]^{\boldsymbol{Ox}}$ are accidentally identical, which is possible but not likely, or $\boldsymbol{L^{Ox}}$ and $[\boldsymbol{L^*}]^{\boldsymbol{Ox}}$ have identical structures. One way around this contradiction is to have a sulfur displaced in $\boldsymbol{L}$ upon oxidation, or

$$L \xrightarrow{IDS} L^{Ox} \rightarrow [L^*]^{Ox} + \left(S^{2-} \quad or \quad HS^-\right) \qquad \text{Eq. (1)}$$

The reaction in Equation (1) is not unexpected. Similar displacements of the “belt” sulfurs (labeled S2B, S3A, and S5A) of the $\boldsymbol{M}$ cluster have been observed.[27] For example, **CO** displaces sulfur S2B under turnover conditions.[28] Selenium has been shown to similarly displace sulfur S2B of the $\boldsymbol{M}$ cluster.[29] Sulfur displacement was also observed in the case of the cofactor ($\boldsymbol{V}$ cluster) of the V-nitrogenase. The $\boldsymbol{V}$ cluster was proposed to have the formula [$VFe_7S_8(CO_3)$●*R-homocitrate*], where CO_3^- has displaced sulfur S3A in that preparation.[30] In addition, a recent x-ray crystallographic analysis of the $\boldsymbol{V}$ cluster under turnover conditions shows a displacement of the sulfur S2B with a bridging $\boldsymbol{OH}$ or $\boldsymbol{NH}$.[31]

The action of sulfur displacement may be important for both substrate reduction[32] and cofactor formation. Lowe and Thorneley ($\boldsymbol{LT}$) formulated a mechanism for the enzymatic N_2 reduction, which is generally accepted today.[1,33,34] In that mechanism, the Fe protein donates electrons ($\boldsymbol{e^-}$), one at a time, to the MoFe protein and, ultimately, to the $\boldsymbol{M}$ cluster in an ATP-driven reaction. A general reduction step of the $\boldsymbol{LT}$ mechanism can be depicted as

$$E_n \xrightarrow{e^- + ATP} E_{n+1} \quad \text{Eq. (2)}$$

where E_n represents the reduction state of one αβ dimer of the tetrameric MoFe protein after receiving n electrons (n = 0 to 7) from the Fe protein. A total of eight electrons are needed for the conversion of one N_2 into two NH_3 plus one H_2. In the ***LT*** scheme, E_0 (S = 3/2) represents the resting state of the protein, an odd-electron (Kramer) reduction state where the ***M*** cluster (M^N) has been reduced by one electron. This state has been well characterized by a large variety of spectroscopic and X-ray crystallographic techniques.[1,5,27,35–38]

The other odd-electron reduction states, E_2 and E_4, are less well characterized but have been predicted to have the ***M*** cluster in the same oxidation state as that in E_0.[39] In other words, the two and four added electrons in states E_2 and E_4, respectively, are not used to reduce the metal cluster but are proposed to have gone into the formation of ***Fe-H-Fe*** hydride bonds in the belt region of the ***M*** cluster.[40]

Finally, very little is known about the even-electron reduced states E_1, and E_3, which are EPR-silent, integer spin states. The one-electron enzymatic reduction of M^N produces M^R in E_1, which has been assumed to represent a reduction of the cofactor itself (i.e., $M^N + e^- \equiv M^R = M^-$). The ***M*** cluster in E_3 is assumed to be at the same oxidation state as that in E_1 (i.e., M^R).[40] As such, during enzymatic turnover, the cofactor is proposed to oscillate between M^N and M^R with each reduction step of the ***LT*** mechanism (Equation 2).[40]

Previously, Mössbauer spectroscopy was used to investigate the M^R cluster in E_1,[41] which showed no major changes in the ***Fe*** isomer shift. This observation suggests that the added electron may not be used to reduce the ***Fe*** atoms in M^R but, by inference, is used to reduce the ***Mo*** atom. This suggestion presents a problem because the oxidation state of ***Mo*** in M^N has recently been proposed to be Mo^{3+},[42] and not Mo^{4+} as previously assumed. Reduction of Mo^{3+} would, therefore, produce Mo^{2+}, which is not a likely scenario. The same Mössbauer spectroscopic study[41] also investigated the ***M*** cluster following radiolytic reduction by gamma radiation to the M^I state. Unlike the results obtained for M^R, significant ***Fe*** isomer shifts were observed for M^I, meaning that the electron was used to reduce the ***Fe*** atoms in M^I. Therefore, the two different reduction procedures result in two different forms of the ***M*** cluster.

The identity of E_1 was recently reinvestigated with Mössbauer as well as ***Mo*** and ***Fe*** X-ray absorption spectroscopies.[43] Those studies showed only small changes in the ***Mo*** X-ray absorption spectrum suggesting that Mo may not change oxidation state in E_1. Curiously, much smaller changes were observed in the ***Fe*** X-ray absorption and Mössbauer spectra but were proposed to correspond to changes in the oxidation state of the ***Fe*** in the cofactor, contrary to the conclusion of the earlier Mössbauer study.

Since all of the ***LT*** mechanistic steps (Equation 2) are reductions, Equation (1), being an oxidation, would seem to have little relevance. However, another definition of M^R, also mentioned in the recent Mössbauer and X-ray absorption study,[43] has been proposed.[39,40] In that scheme, E_1 contains a ***Fe-H-Fe*** hydride bridge similar to that proposed for E_2. Since

hydride bonds require two electrons while $\boldsymbol{E_1}$ has received only one electron from the Fe protein, the second electron is proposed to come from the ***M*** cluster, resulting in an oxidation (yielding $\boldsymbol{M^+}$) rather than reduction (yielding $\boldsymbol{M^-}$) as previously thought, or

$$M^N \xrightarrow{e^- + H^+} M^R = \left(M^+ - \mathrm{H}^-\right) \quad \text{Eq. (3)}$$

If Equation (3) is correct, then Equation (1) may be instrumental in enzymatic activity assuming, of course, that the ***M*** cluster behaves similarly in response to oxidation to the ***L*** cluster. In that situation, enzymatic reduction of $\boldsymbol{E_0}$ to $\boldsymbol{E_1}$ (or $\boldsymbol{E_2}$ to $\boldsymbol{E_3}$) would result in an oxidized ***M*** cluster, making the belt sulfur more labile and, therefore, more easily displaced by an inhibitor or substrate. For example, the mechanism for ***CO*** binding could be written as

$$\begin{aligned} &M^N \xrightarrow{e^- + H^+} \left(M^+ - H^-\right) \xrightarrow{CO} \left(CO{-}[M^*]^+ - H^-\right) \\ &+ S^{2-} \xrightarrow{e^- + H^+} (CO{-}M^*) + H_2 + S^{2-} \end{aligned} \quad \text{Eq. (4)}$$

repeatedly followed by

$$(CO{-}M^*) \xrightarrow{e^- + H^+} \left(CO{-}[M^*]^+ - H^-\right) \xrightarrow{e^- + H^+} (CO{-}M^*) + H_2 \quad \text{Eq. (5)}$$

where ***CO*** has replaced (or displaced) a belt sulfur (S2B), and ***M****, like ***L****, represents the ***M*** cluster minus one sulfur. This mechanism also suggests that ***CO*** functions as a non-competitive enzymatic inhibitor because its binding to the cofactor blocks the formation of a second hydride (***Fe-H-Fe***), a hydride that has been proposed to be a central part of $\boldsymbol{N_2}$ binding.[40] Therefore, CO binding only allows $\boldsymbol{H_2}$ production to occur (Equation 5). It should be noted, however, that alternative explanations for CO being a non-competitive inhibitor of N_2 may be found in scenarios in which CO and N_2 bind at different locations or use different mechanisms for binding and/or reduction. In addition, electron acceptors other than H^+ may be used to “park” the electrons derived from the Fe protein and the M-cluster, although formation of the hydride-bound species is an appealing proposal from a chemical perspective.

Regardless, the general mechanism proposed in Equation 4 could also be applied to interpreting the outcome of the recent X-ray crystallographic study of V-nitrogenase,[31] which has revealed that sulfur S2B becomes labile under turnover conditions and can be removed reversibly from the ***V*** cluster. The decrease in the total EPR spectrum and absence of any new EPR signal in the turnover sample suggests that the VFe protein crystal may be poised in an even-electron reduced state, likely $\boldsymbol{E_1}$. [31,32] In this case, the belt sulfur (S2B) may become labile upon a one-electron reduction of the protein and is replaced by either ***OH*** or ***NH***.

Equation (1) may also be applied to ***L*** cluster maturation. The introduction of the final 9th sulfur to produce ***L*** requires an oxidized form of sulfur (i.e., $\boldsymbol{SO_3^{2-}}$), while a reduced form (e.g., $\boldsymbol{S^{2-}}$) does not support sulfur insertion.[17] Similarly, ***Se*** exchange with sulfur on the ***M*** cluster occurs with the oxidized $\boldsymbol{SeCN^-}$ form but not the reduced $\boldsymbol{Se^{2-}}$ form.[29] Therefore,

these insertion/exchange reactions can be viewed as oxidation-induced reactions where SO_3^{2-} or $SeCN^-$ oxidize the ***L**** or ***M*** cluster, opening the structure and thereby making the cluster more favorable to the eventual insertion or exchange of the reduced S^{2-} or Se^{2-}.

In summary, even though the ***L*** and ***L**** clusters have different structures, the oxidized forms of these clusters (L^{Ox} and $[L^*]^{Ox}$, respectively) exhibit essentially identical EPR and MCD spectra. Furthermore, the magnetization curves of the L^{Ox} and $[L^*]^{Ox}$ clusters are basically identical. These data suggest that a belt sulfur of the ***L*** cluster is displaced upon oxidation, making the L^{Ox} and $[L^*]^{Ox}$ clusters identical, thus explaining why their spectra are nearly indistinguishable. While it is as-of-yet unclear whether a similar oxidation-induced migration of sulfur also occurs on the ***M*** cluster, oxidation of the ***M*** cluster (Equation 3) could make the belt sulfur more labile to migration, especially in the presence of an inhibitor or substrate. Therefore, sulfur migration may have an important mechanistic role in substrate or inhibiter binding.[32] The proposal presented herein is that enzymatic inhibitor or substrate binding occurs at the EPR-silent E_1 or E_3 state that involves an oxidized ***M*** cluster (and not a reduced ***M*** cluster as previously thought) with a labilized belt region. Ongoing experiments will shed further light on this proposal in hopes of contributing to a better understanding of the biosynthetic and catalytic mechanisms of nitrogenase.

Experimental Section

Unless otherwise noted, all chemicals were purchased from Sigma-Aldrich and Thermo-Fisher Scientific.

Cell Growth and Protein Purification.

The *Escherichia coli* strain (YM114EE) expressing a His-tagged form of NifB from *Methanosarcina acetivorans* (*Ma*NifB) was grown and harvested as described previously.[15] Subsequently, *Ma*NifB was purified using published methods.[15]

Cluster Reconstitution and Sulfur Insertion.

The as-isolated *Ma*NifB protein was reconstituted with a synthetic $[Fe_4S_4]$ cluster ($[PPh_4]_2[Fe_4S_4(SCH_2CH_2OH)_4]$) in the presence of europium(II) ethyleneglycol-bis(2-aminomethylether)-*N,N,N',N'*-tetraacetic acid (Eu^{II}-EGTA) as described earlier.[16] Subsequently, the reconstituted *Ma*NifB (carrying the ***K*** cluster) was matured in the presence of SAM, with or without sodium sulfite (Na_2SO_3), to yield *Ma*NifB proteins carrying the ***L*** and ***L**** clusters, respectively, as described previously.[17]

EPR Analysis.

EPR samples were prepared under Ar in a Vacuum Atmospheres glove box (operating at <3 ppm O2) and flash frozen in liquid nitrogen prior to analysis. The IDS-oxidized sample was prepared by incubating *Ma*NifB bound with either the L-cluster or the L*-cluster with excess IDS for 5 min, followed by removal of excess IDS with a Sephadex G-25 desalting column. X-band EPR spectra were recorded on an ESP 300 Ez spectrophotometer (Bruker) interfaced with an ESR-9002 liquid-helium continuous-flow cryostat (Oxford Instruments) using a microwave power of 50 mW, a gain of 5×10^4, a modulation frequency of 100 kHz,

and a modulation amplitude of 5 G. Four scans were recorded for each sample at a temperature of 10 K and a microwave frequency of 9.62 GHz. W-band spectra were recorded on a home-built instrument at the Electron Magnetic Resonance Facility at the High Magnetic Field Laboratory of Florida State University in Tallahassee, FL., using a microwave power of 50 mW and a modulation amplitude of 1 mT. Samples were recorded at a temperature of 10 K and a microwave frequency of 94 GHz.

MCD Spectroscopy.

MCD samples were prepared as described above for EPR spectroscopy, followed by transfer of samples to MCD cuvettes (each holding ~160 μL sample) constructed of optical quality quartz (Model 1Q1, 1mm path length, Starna Cells Inc.; Atascadero, CA) and cut to the appropriate dimensions to fit the sample holder (2.0 cm × 12.5 mm, 1 mm internal path length). Subsequently, the MCD cuvettes were frozen in liquid nitrogen/pentane slush. All samples contained 50% glycerol to ensure the formation of an optical glass upon freezing, and were kept on dry ice during transit.

MCD spectroscopy was performed with a modified CD spectropolarimeter (JASCO: Model J-715) interfaced with a superconducting magnet (Oxford: Model Spectromag 400–7T). Sample temperatures were monitored with two thin film resistance temperature sensors (Lakeshore: Cenox: Model CX1050-Cu-1–4L) positioned directly above (1 mm) and below (1 mm) the sample cuvette. The linearity of the magnetic field was monitored with a calibrated Hall generator (Lakeshore: Model HGCA-3020) placed directly outside the superconducting magnet. MCD spectra were recorded at a rate of 50 nm min^{-1} and a resolution of 10 nm using a photomultiplier with a spectral range of 200–900 nm. Since optical glasses formed at low temperatures often generate a strain-induced background, the CD spectrum was recorded in zero magnetic field to determine whether the background signal was excessive. To eliminate interference by any background CD signal, the corrected MCD spectrum was obtained for each sample by first recording the spectrum with the magnetic field in the normal direction and subsequently subtracting from it the spectrum with the field in the reversed direction. All spectral intensities were corrected for path length and sample concentration.

MCD spectral intensities are the composite of three additive, contributing terms, called **A**, **B**, and **C**. The **A**-term arises from degenerate excited states, while the **C**-term arises from degenerate ground states. The **B**-term contribution does not require any degeneracy and is often temperature independent. The **C**-term is dependent on ground state degeneracy and its intensity is regulated by the Boltzmann distribution of that state such that the intensity decreases with increasing temperature.

Analysis of Magnetization Data.

Magnetization curves are plots of the fractional intensity increase as a function of $\beta B/2kT$, where β is the Bohr magneton, B is the magnetic field flux, k the Boltzmann constant, and T is the absolute temperature. Curves were recorded at a set wavelength and different temperatures, while the magnetic field was linearly varied from 0–6 T at a rate of 0.1 A/s with a resolution of 2 s. MCD data were analyzed using a fit/simulation program.[26] The

program allows the calculation of best-fit saturation magnetization curves using experimental data as a basis set and is valid for any spin state, half-integer or integer, at any specified temperature.

Experimental data were analyzed by fitting the Spin Hamiltonian parameters and the effective transition moment products, M_{xy}^{eff}, M_{xz}^{eff} and M_{yz}^{eff}, with a scaling parameter $A_{satlim} = /\gamma S$, where γ is the magnetogyric ratio. The effective transition moment products represent the planes of polarization that reflect the anisotropy of the *g*-factors. Since the initial slope of the magnetization curve is dependent on the *g*-factors, the transition polarizations relate the transition dipole to the *g*-factor axes of a powder or randomly-oriented sample.

Acknowledgements

This work was supported by NIH-NIGMS grant GM67626 (to M.W.R. and Y.H.).

References

[1]. Burgess BK; Lowe DJ, Chem. Rev 1996, 96, 2983–3011. [PubMed: 11848849]

[2]. Kim J; Rees DC, Science 1992, 257, 1677–1682. [PubMed: 1529354]

[3]. Kim J; Rees DC, Nature 1992, 360 (10), 553–560. [PubMed: 25989647]

[4]. Chan MK; Kim J; Rees DC, Science 1993, 260, 792–794. [PubMed: 8484118]

[5]. Rees DC; Kim J; Woo D, Biochemistry 1993, 32, 7104–7115. [PubMed: 8393705]

[6]. Kim J; Rees DC, Biochemistry 1994, 33 (2), 389–397. [PubMed: 8286368]

[7]. Lancaster KM; Hu Y; Bergmann U; Ribbe MW; DeBeer S, J. Am. Chem. Soc 2013, 135, 610–612. [PubMed: 23276198]

[8]. Spatzal T; Aksoyoglu M; Zhand L; Andrade SLA; Schleicher E; Weber S; Rees DC; Einsle O, Science 2011, 334, 940. [PubMed: 22096190]

[9]. Wiig JA; Hu Y; Ribbe MW, Proc. Natl. Acad. Sci. U. S. A 2011, 108, 8623–8627. [PubMed: 21551100]

[10]. Hu Y; Ribbe MW, Annu. Rev. Biochem 2016, 85, 455–483. [PubMed: 26844394]

[11]. Sickerman NS; Ribbe MW; Hu Y, Acc. Chem. Res 2017, 50 (11), 2834–2841. [PubMed: 29064664]

[12]. Hu Y; Ribbe MW, Curr. Opin. Chem. Biol 2016, 31, 188–194. [PubMed: 26969410]

[13]. Hu Y; Corbett MC; Fay AW; Webber JA; Hodgson KO; Hedman B; Ribbe MW, Proc. Natl. Acad. Sci. U. S. A 2006, 103 (46), 17119–17124. [PubMed: 17050696]

[14]. Kaiser JT; Hu Y; Wiig JA; Rees DC; Ribbe MW, Science 2011, 331, 91–94. [PubMed: 21212358]

[15]. Fay AW; Wiig JA; Lee CC; Hu Y, Proc. Natl. Acad. Sci. U. S. A 2015, 112 (48), 14829–14833. [PubMed: 26627238]

[16]. Rettberg LA; Wilcoxen J; Lee CC; Stiebritz MT; Tanifuji K; Britt RD; Hu Y, Nat. Comm 2018, 9, 2824–2832.

[17]. Tanifuji K; Lee CC; Sickerman NS; Tatsumi K; Ohki Y; Hu Y; Ribbe MW, Nat. Chem 2018, 10, 568–572. [PubMed: 29662207]

[18]. Jasniewski AJ; Wilcoxen J; Tanifuji K; Hedman B; Hodgson KO; Britt RD; Hu Y; Ribbe MW, Angew. Chem. Int. Ed. Engl 2019, 58, 14703–14707. [PubMed: 31411369]

[19]. Rupnik K; Hu Y; Fay AW; Ribbe MW; Hales BJ, J. Biol. Inorg. Chem 2011, 16, 325–332. [PubMed: 21038112]

[20]. Fay AW; Blank MA; Lee CC; Hu Y; Hodgson KO; Hedman B; Ribbe MW, Angew. Chem. Int. Ed. Engl 2011, 50, 7787–7790. [PubMed: 21726031]

[21]. Guo Y; Echavarri-Erasun C; Demuez M; Jimenez-Vincente E; Bominaar E; Rubio LM, Angew. Chem. Int. Ed. Engl 2016, 55 (41), 12764–12767. [PubMed: 27611968]

[22]. Yoshizawa J; Blank MA; Fay AW; Lee CC; Wiig JA; Hu Y; Hodgson KO; Hedman B; Ribbe MW, J. Am. Chem. Soc 2009, 131, 9321–9325. [PubMed: 19514721]

[23]. Fay AW; Blank MA; Rebelein JG; Lee CC; Ribbe MW; Hedman B; Hodgson KO; Hu Y, Proc. Natl. Acad. Sci. U. S. A 2016, 113 (34), 9504–9508. [PubMed: 27506795]

[24]. Johnson MK; Thomson AJ; Robinson AE; Smith BE, Biochim. Biophys. Acta 1981, 671, 61–70.

[25]. Morningstar JE; Johnson MK; Case EE; Hales BJ, Biochemistry 1987, 26 (7), 1795–1800. [PubMed: 3474027]

[26]. Neese F; Solomon EI, Inorg. Chem 1999, 38, 1847–1865. [PubMed: 11670957]

[27]. Einsle O; Tezca FA; Andrade SLA; Schmid B; Yoshida M; Howard JB; Rees DC, Science 2002, 297, 1696–1700. [PubMed: 12215645]

[28]. Spatzal T; Perez K; Einsle O; Howard JB; Rees DC, Science 2014, 345 (6204), 1620–1623. [PubMed: 25258081]

[29]. Spatzal T; Perez K; Howard JB; Rees DC, Elife 2015, 4, e11620. [PubMed: 26673079]

[30]. Sippel D; Einsle O, Nat. Chem. Biol 2017, 13, 956–960. [PubMed: 28692069]

[31]. Sippel D; Rohde M; Netzer J; Trncik C; Gies J; Grunau K; Djurdjevic I; Decamps L; Andrade SLA; Einsle O, Science 2018, 359, 1484–1489. [PubMed: 29599235]

[32]. Skubi K; Holland PL, J. Am. Chem. Soc 2018, 57, 3540–3541.

[33]. Thorneley RNF; Lowe DJ, Biochem. J 1984, 224, 877–886. [PubMed: 6395861]

[34]. Thorneley RNF; Lowe DJ, Israel Journal of Botany 1982, 31, 61–71.

[35]. Hoffman BM; Roberts JE, J. Am. Chem. Soc 1982, 104 (3), 860–862.

[36]. Hoffman BM; Venters RA; Roberts JE, J. Am. Chem. Soc 1982, 104, 4711–4712.

[37]. Lindahl PA; Gorelick NJ; Münck E; Orme-Johnson WH, J. Biol. Chem 1987, 262, 14945–14953. [PubMed: 2822707]

[38]. Lindahl PA; Papaefthymiou V; Orme-Johnson WH; Münck E, J. Biol. Chem 1988, 263 (36), 19412–19418. [PubMed: 2848826]

[39]. Seefeldt LC; Hoffman BM; Dean DR, Curr. Opin. Chem. Biol 2012, 16, 19–25. [PubMed: 22397885]

[40]. Hoffman BM; Lukoyanov D; Yang Z-Y; Dean DR; Seefeldt LC, Chem. Rev 2014, 114, 4041–4062. [PubMed: 24467365]

[41]. Yoo SJ; Angove HC; Papafthymiou V; Burgess BK; Münck E, J. Am. Chem. Soc 2000, 122, 4926–4936.

[42]. Bjornsson R; Lima FA; Spatzal T; Weyhermuller T; Glatzel P; Bill E; Einsle O; Neese F; DeBeer S, Chem. Sci 2014, 5, 3096–3103.

[43]. Van Stappen C; Davydov R; Yang Z-Y; Fan R; Guo Y; Bill E; Seefeldt LC; Hoffman BM; DeBeer S, Inorg. Chem 2019, 58, 12365–12376. [PubMed: 31441651]

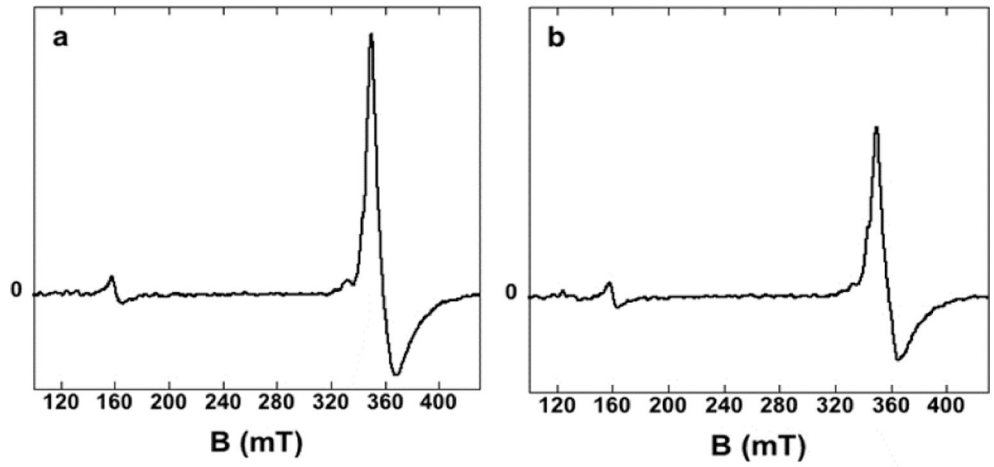

Figure 1.

Perpendicular mode X-band spectra of *Ma*NifB-bound $\boldsymbol{L^{Ox}}$ (a) and $[\boldsymbol{L*}]^{\boldsymbol{Ox}}$ (b) recorded at a temperature of 10 K, a modulation amplitude of 1 mT, a microwave power of 50 mW and a microwave frequency of 9.62 GHz. The sample concentrations are 19 mg/mL ($\boldsymbol{L^{Ox}}$) and 19.1 mg/mL ($[\boldsymbol{L*}]^{\boldsymbol{Ox}}$). The small signal at *ca.* 160 mT likely arises from a minor concentration of adventitious hexa-aquo $\boldsymbol{Fe^{3+}}$ ($S = 5/2$).

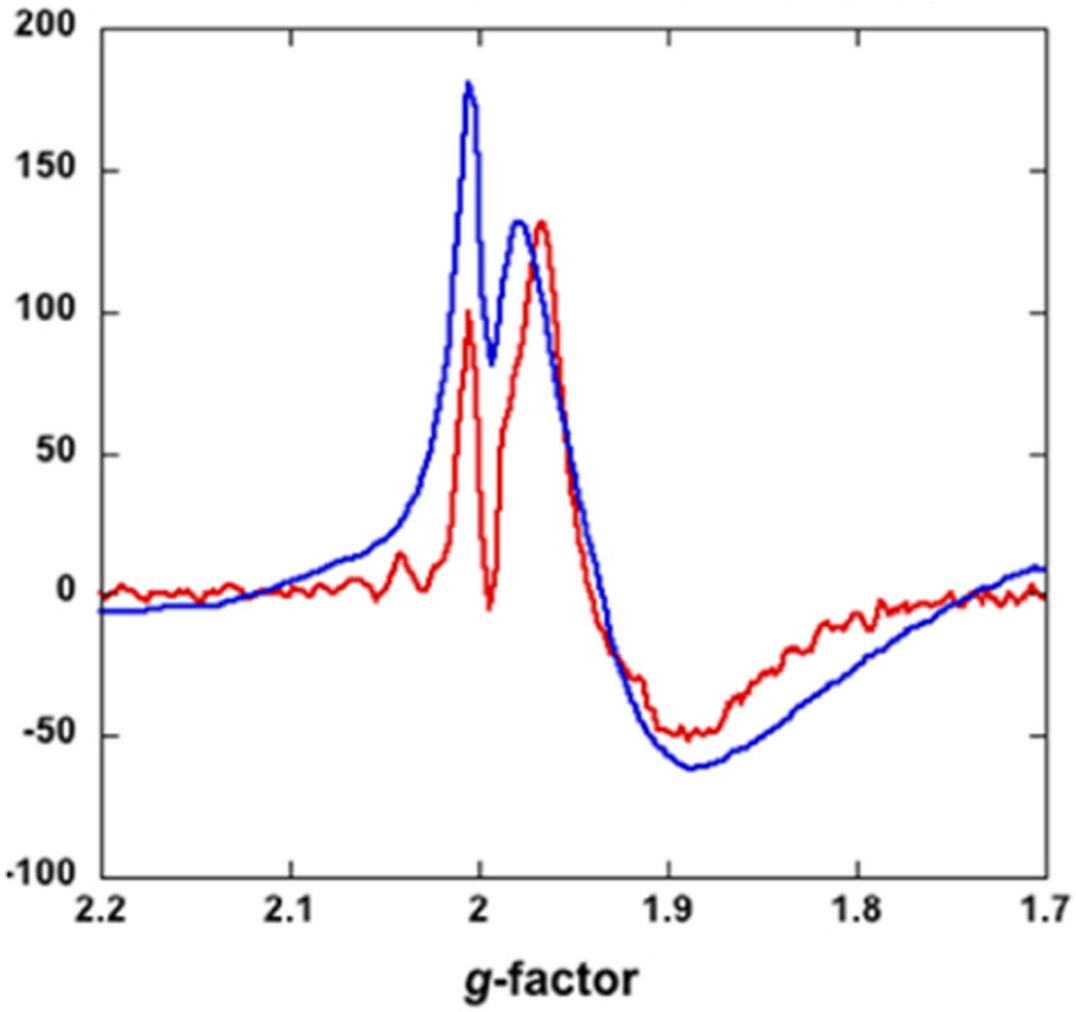

Figure 2.

The spectra of the $\boldsymbol{L^{Ox}}$ cluster recorded at X- band (9.62 GHz; blue) and W-band (94 GHz; red) frequencies. A comparison of these spectra shows that an increase in microwave frequency does not improve resolution. This is due to a near-linear increase in linewidth with frequency. The sharp signal at $g \sim 2$ originates from a minor $S = 1/2$ radical impurity. Both X- and W-band spectra were recorded at a temperature of 10 K, a modulation amplitude of 1 mT and a microwave power of 50 mW.

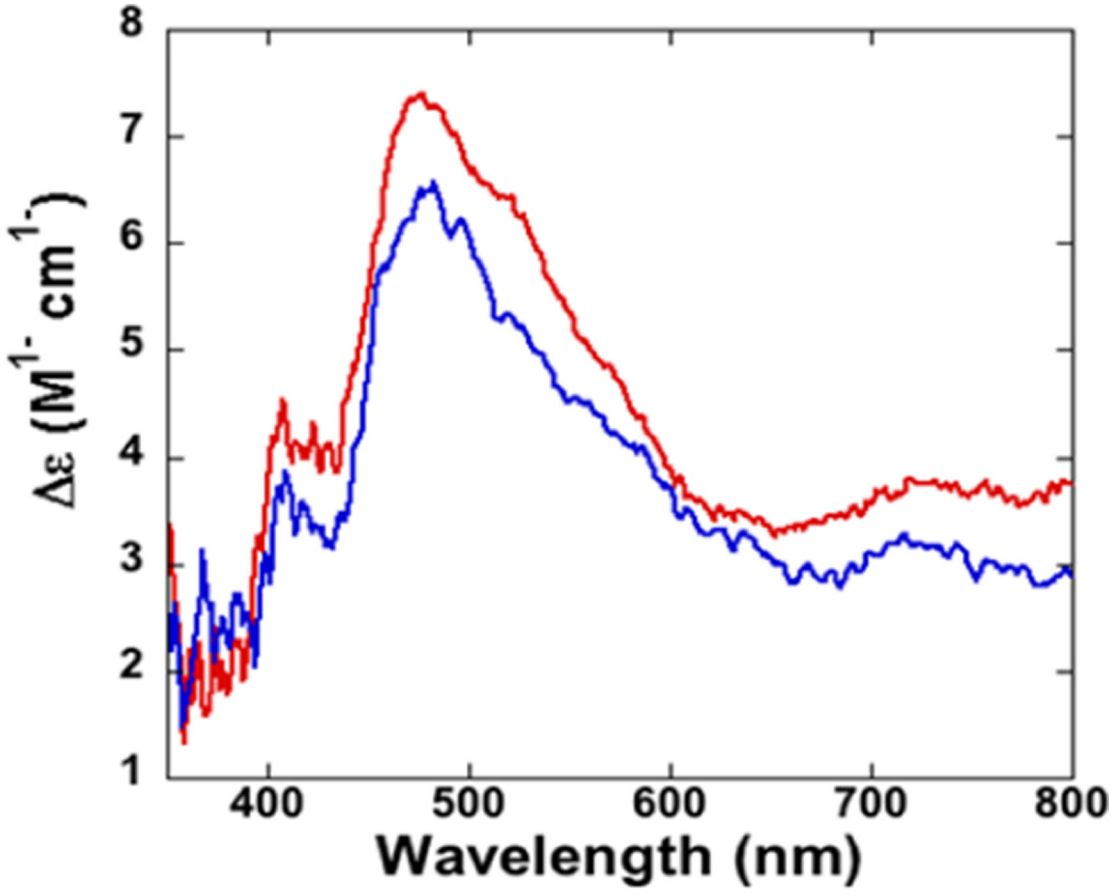

Figure 3.

The MCD spectra of *Ma*NifB-bound $\boldsymbol{L^{Ox}}$ (blue) and $[\boldsymbol{L^{*}}]^{\boldsymbol{Ox}}$ (red) recorded at a temperature of 1.4 K and a magnetic field of 6 T. The sample concentrations are 19 mg/mL ($\boldsymbol{L^{Ox}}$) and 19.1 mg/mL ($[\boldsymbol{L^{*}}]^{\boldsymbol{Ox}}$).

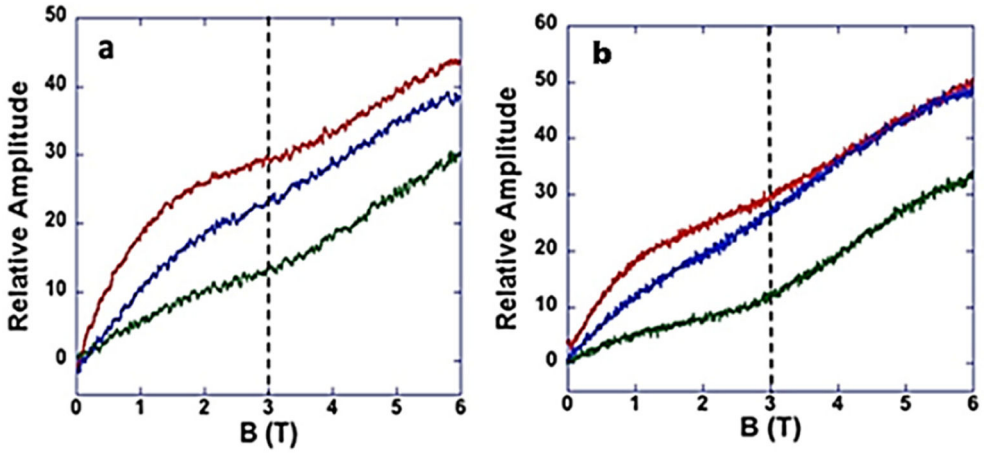

Figure 4.

Amplitude of the MCD spectra of $\boldsymbol{L}^{Ox}$ (a) and $[\boldsymbol{L}*]^{Ox}$ (b) at 480 nm and at 1.4 K (red), 4.2 K (blue) and 13 K (green). The vertical dashed black lines represent the approximate fields where the amplitudes make an upward break.

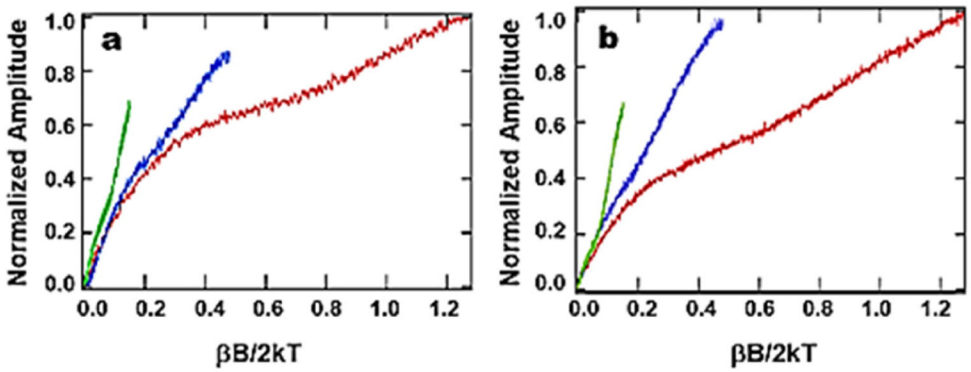

Figure 5.

Plots showing the magnetization curves of $\boldsymbol{L^{Ox}}$ (a) and $\boldsymbol{(L^{*})^{Ox}}$ (b) versus $\boldsymbol{\beta B/2kT}$ at T = 1.6 K, 4.2 K and 10 K. Attempts at simulating all data were unsuccessful, mainly due to the atypical upward curve of the data at ca. 3 T. It is interesting to note, however, that both sets of data are temperature independent at low values of $\boldsymbol{\beta B/2kT}$, suggesitng $S = 1/2$. The deviation from this trend at higher $\boldsymbol{\beta B/2kT}$ values is unexplained, but this deviation is definely not due to a diamagnetic (i.e., ***B***-term) contribution.